CMS Physics Analysis Summary

Contact: cms-pag-conveners-susy@cern.ch 2018/09/17

Search for the pair production of light top squarks in the eμ final state in proton-proton collisions at $\sqrt{s} = 13$ TeV

The CMS Collaboration

Abstract

A search for the production of a pair of top squarks in proton-proton collisions at the CERN LHC is presented. This search targets a region of the parameter space where the kinematics of top squark pair production and top quark pair production are very similar, due to the mass of the neutralino being small. The search is performed with 36.9 fb^{-1} of proton-proton collisions collected by the CMS detector, using events containing one opposite-sign electron-muon pair. The search is based on a precise estimation of the $\mathrm{t\bar{t}}$ background, and the use of the M_{T2} variable that combines the transverse mass of each lepton and the missing transverse energy. No excess of events is found over the standard model predictions and exclusion limits are placed at 95% confidence level on the production of top squarks up to masses of 200 GeV for models with $m_{\tilde{\mathrm{t}}_1} - m_{\tilde{\chi}_1^0} \simeq m_{\mathrm{top}}$.

1 Introduction

The standard model (SM) accurately describes the vast majority of the known particle physics phenomena. However, there are several open questions that cannot be explained by the SM, prominent among them being the hierarchy problem between the Higgs mass and the Planck scale [1, 2], or the lack of a candidate particle that explains the composition of the dark matter in cosmological observations [3, 4]. Supersymmetry (SUSY) [5–13] is a well-motivated extension of the SM that provides a natural solution to these problems through the introduction of an additional symmetry between bosons and fermions. In SUSY models, a large quantum loop correction to the mass of the Higgs bosons, mainly produced by the top quark, can be compensated by the one produced by the top squark, resulting in a natural solution if the masses of the two particles are of the same order. Furthermore, if R-parity is conserved [14], top squarks are produced in pairs and the lightest supersymmetric particle (LSP) is stable so it becomes a good candidate for dark matter. The lighter SUSY particles may have masses close to the SM particles, and therefore could be produced in proton-proton collisions within the energy reach of the CERN LHC. In particular, in some scenarios the lightest top squarks are expected to have a mass ($m_{\tilde{t}_1}$) close to the top quark mass (m_{top}), for a natural solution to the hierarchy problem [15, 16].

This note presents a search for the production of a pair of scalar top partners that are degenerate or nearly degenerate with top quarks ($m_{\tilde{t}_1}$- $m_{\tilde{\chi}^0_1} \simeq m_{\text{top}}$), using events with an opposite-sign electron-muon pair produced in pp collisions at a centre-of-mass energy of $\sqrt{s} = 13$ TeV and recorded with the CMS detector at the CERN LHC. A total integrated luminosity of 35.9 fb^{-1} of data, collected during 2016, is used.

The degenerate and nearly degenerate top squarks in this search are assumed to decay as $\tilde{t}_1 \rightarrow t\,\tilde{\chi}^0_1$, as shown in Fig. 1. In particular, this analysis uses events in which the resulting top quark and antiquark decay into a b quark and a W boson which in turn decays into a lepton and a neutrino, and selects final states characterized by the presence of an electron and a muon.

Given that the target SUSY signal and the SM $t\bar{t}$ production process are characterized by final states with very similar kinematics, most dedicated searches by the ATLAS [17–21] and CMS [22–27] Collaborations do not have enough sensitivity to set exclusion limits to the production of top squarks with these masses. Limits on the production cross section of signals described by these models have previously been set through $t\bar{t}$ production cross section measurements at 8 TeV by the CMS [28] and ATLAS [29] Collaborations, excluding the presence of a top squark with a mass of up to 183 GeV for a neutralino mass of 1 GeV.

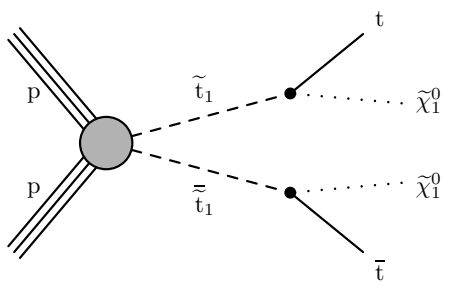

Figure 1: Diagram of the top squark-antisquark production with further decay into a top quark and the lightest neutralino.

In the search presented in this note, a precise estimation of the $t\bar{t}$ background production rate

is performed, so the SUSY signal can be detected as an excess above the prediction. Further discrimination is achieved by exploiting the distribution of signal and background events in a discriminating variable.

2 The CMS detector

The main feature of the CMS detector is a superconducting solenoid that provides an axial magnetic field of 3.8 T. A silicon pixel and a strip tracker measure the trajectory of charged particles, covering the full range of the azimuthal angle $0 < \varphi < 2\pi$, and a pseudorapidity of $|\eta| < 2.5$. A lead tungstate crystal electromagnetic calorimeter and a brass and scintillator hadron calorimeter are located inside the solenoid and used to identify electrons, photons and jets. Muons are detected in gas-ionization detectors embedded in the magnet steel flux-return yoke outside the solenoid.

Extensive forward calorimetry complements the coverage provided by the barrel and endcap detectors that improve the measurement of the imbalance in transverse momentum. The detector is nearly hermetic, providing reliable measurement of the momentum imbalance in the plane transverse to the beams. A two-level trigger system selects the most interesting pp collisions for offline analysis.

A more detailed description of the CMS detector, together with a definition of the coordinate system used and the relevant kinematic variables, can be found in Ref. [30].

3 Monte Carlo simulation

The POWHEG v2 [31] generator is used to simulate $\mathrm{t\bar{t}}$ events at the next-to-leading-order in QCD (NLO), as well as the dependency of the $\mathrm{t\bar{t}}$ production on m_{top}, factorization (μ_{F}), and renormalization (μ_{R}) scales. A parameter, denoted as damping parameter h_{damp}, is used to limit the resummation of higher order effects by the Sudakov form factor to below a given p_{T} scale [32].

Single top quark and antiquark production in association with a W boson (tW) is simulated at NLO using POWHEG v1 [33]. The Drell-Yan process (DY), W and Wγ background samples, as well as the production of W and Z bosons in association with $\mathrm{t\bar{t}}$ events (referred to as $\mathrm{t\bar{t}V}$) are generated at NLO using the MG5_aMC@NLO v2.2.2 [34] generator. The production of Z bosons is simulated with up to two additional partons and the FxFx scheme is used for the merging of the matrix elements [35]. The contributions from WW, WZ, and ZZ (collectively referred to as VV) processes are simulated at leading-order (LO) using PYTHIA v8.205 [36].

The generation of signal samples is performed using MG5_aMC@NLO with the same generation parameters as the $\mathrm{t\bar{t}}$ background sample, to avoid introducing a bias from the generation of the samples in the search.

The NNPDF 3.0 [37] parton distribution functions (PDF) set is used for all the samples (LO and NLO generators). Parton showering and hadronization are handled by PYTHIA v8.205 using the underlying event tune CUETP8M2T4 [38] for $\mathrm{t\bar{t}}$ events and the CUETP8M1 [39] tune for all the other background and signal events.

The response of the CMS detector is simulated for all the generated events with the GEANT4 package [40]. The effect of additional interactions in the same bunch crossing (referred to as pileup) is accounted for by simulating additional interactions for each hard scattering event.

Simulated events are then reweighted so that the pileup distribution matches that observed in data, which is characterized by an average of 27 collisions per bunch crossing.

Simulated events are normalized according to the integrated luminosity and the theoretical cross sections of each process. The latter are computed at next-to-next-to-leading order (NNLO) (W+jets and DY [41]), approximate next-to-next-to-leading order (aNNLO) (tW [42]), and NLO (diboson [43]).

For the simulated $\mathrm{t\bar{t}}$ sample, the full NNLO plus next-to-next-to-leading-logarithmic accuracy calculation [44], performed with the TOP++ 2.0 program [45], is used. PDF uncertainties are added in quadrature to the uncertainty associated with the strong coupling constant (α_s) to obtain a $\mathrm{t\bar{t}}$ production cross section of $832\,^{+20}_{-29}$ (scale) ± 35 (PDF+α_s) pb assuming $m_{\mathrm{top}} = 172.5$ GeV.

The signal events are normalized to the calculated theoretical NLO cross section [46].

4 Object and event selection

The top quarks coming from the decay of the top squarks decay almost exclusively into a b quark and a W boson. In this analysis, events containing an $\mathrm{e}^{\pm}\mu^{\mp}$ pair and jets are selected. Signal events may have a larger amount of missing transverse momentum with respect to $\mathrm{t\bar{t}}$ events due to the presence of the neutralinos.

Events are required to pass a dilepton trigger based on the presence of one electron (muon) with transverse momentum $p_{\mathrm{T}} > 12$ (8) GeV and one muon (electron) with $p_{\mathrm{T}} > 23$ GeV, or a single-lepton trigger that requires the presence of one electron (muon) with $p_{\mathrm{T}} > 27$ (24) GeV. The efficiency of the combined triggers is measured in data and found to be approximately 98%. The efficiency of the simulated trigger is corrected to match that observed in data by using a multiplicative scale factor (SF) calculated as a function of the pseudorapidity of the leptons.

The particle-flow (PF) algorithm [47] is used to reconstruct and identify each individual particle in the event by combining the information from all the CMS subdetectors. Electrons are identified as a primary charged particle track and potentially many ECAL energy clusters corresponding to this track extrapolation to the ECAL and to possible bremsstrahlung photons emitted along the way through the tracker material. Muons are identified as a track in the central tracker consistent with either a track or several hits in the muon system, associated with an energy deficit in the calorimeters. Selected leptons are required to have $p_{\mathrm{T}} \geq 20$ GeV, $|\eta| < 2.4$, and to satisfy a lepton isolation criterion. The lepton isolation variable is defined as the scalar sum of the transverse momenta of all the PF candidates inside a cone of $\Delta R = \sqrt{(\Delta\eta)^2 + (\Delta\phi)^2} = 0.3$ (0.4) centered on the electron (muon) candidate, excluding the contribution from the lepton candidate itself. This isolation variable is required to be smaller than 6 (15)% of the electron (muon) candidate p_{T}.

Jets are reconstructed from PF candidates using the anti-$\mathrm{k_T}$ clustering algorithm [48, 49] with a distance parameter of 0.4. The jet momentum is defined as the vectorial sum of the momenta of all PF candidates associated to the jet, and is found to be within 5–10% of the true momenta over the whole p_{T} spectrum. PF candidates that are determined to be originating from pileup vertices are discarded in the jet reconstruction, and an offset correction is applied to account for remaining contributions of the pileup interactions. Selected jets are required to have $p_{\mathrm{T}} \geq 30$ GeV and $|\eta| < 2.4$. In order to avoid double counting, jets that overlap with the selected leptons in a cone of $\Delta R = 0.4$ are not considered.

Jets originating from b quarks are identified (tagged) as b jets using the combined secondary vertex algorithm v2 [50], with an operating point that yields identification efficiencies of about 70%; the corresponding misidentification probabilities are about 1% for light-flavour jets (originating from u, d, s quarks or gluons) and 15% for c jets.

Muons are measured in the pseudorapidity range $|\eta| < 2.4$, with detection planes made using three technologies: drift tubes, cathode strip chambers, and resistive plate chambers. Matching muons to tracks measured in the silicon tracker results in a relative transverse momentum resolution for muons with $20 < p_T < 100\,\text{GeV}$ of 1.3–2.0% in the barrel and better than 6% in the endcaps. The p_T resolution in the barrel is better than 10% for muons with p_T up to 1 TeV [51].

The electron momentum is estimated by combining the energy measurement in the ECAL with the momentum measurement in the tracker. The momentum resolution for electrons with $p_T \approx 45\,\text{GeV}$ from $Z \to ee$ decays ranges from 1.7% for nonshowering electrons in the barrel region to 4.5% for showering electrons in the endcaps [52].

Lepton reconstruction, identification, and isolation efficiencies, as well as efficiencies for b tagging and b tag misidentification of light quarks or gluons, are corrected in the MC simulation to match the values observed in data. These corrections are parameterized as functions of p_T and η and are of the order of ≈1% for leptons and ≈10% for jets.

The vectorial missing transverse momentum ($\vec{p}_T^{\,\text{miss}}$) is defined as the transverse component of the negative vectorial sum of the momenta of all reconstructed PF candidates in an event; its magnitude is denoted as p_T^{miss} and referred to as missing transverse momentum. All the corrections applied to the jet momenta are propagated to the calculation of p_T^{miss} [53].

Events containing one electron-muon pair with opposite charge and invariant mass greater than 20 GeV are selected. The highest-p_T lepton must be at least of 25 GeV. In case more than two leptons are present in the event, the dilepton pair is formed using the two highest-p_T leptons, and the event is selected if that pair satisfies the aforementioned requirements. Selected events are also required to contain at least two jets and at least one b-tagged jet.

5 Search strategy

After the event selection, the vast majority of events (≈98%) come from top quark production processes ($t\bar{t}$, tW). For top squark masses similar to that of the top quark, the production cross section of signal processes amounts to up to 125 pb, corresponding to about 15% of the SM $t\bar{t}$ production cross section, but the kinematics of the final state particles are very similar in both processes, so a control region for the $t\bar{t}$ background with small signal contamination is impossible to define. The sensitivity of the analysis comes from a precise estimate of the $t\bar{t}$ background, using MC simulation and taking into account that its theoretical uncertainties on the cross section are of the order of about 6% [45] and the experimental uncertainties are even smaller [28, 54]. Additional sensitivity comes from the exploitation of kinematic differences between the target signal and the $t\bar{t}$ background.

For a top squark mass of 245 GeV, the cross section of the process decreases to ≈24 pb, but the presence of massive neutralinos (>50 GeV) in the event results in additional p_T^{miss}. To account for this, following previous top squark searches [25] the sensitivity of the analysis is further increased by using the shape of the M_{T2} variable, defined as:

$$M_{T2}^2 = \min_{\vec{p}_{T1}^{\,miss} + \vec{p}_{T2}^{\,\text{miss}} = \vec{p}_T^{\,\text{miss}}} \left(\max \left[m_T^2(\vec{p}_T^{\,\ell 1}, \vec{p}_{T1}^{\,\text{miss}}), m_T^2(\vec{p}_T^{\,\ell 2}, \vec{p}_{T2}^{\,\text{miss}}) \right] \right) \quad (1)$$

where m_{T}^2 is the squared transverse mass and $\vec{p}_{\mathrm{T1}}^{\,\mathrm{miss}}$, $\vec{p}_{\mathrm{T2}}^{\,\mathrm{miss}}$ correspond to the transverse momentum of two neutrinos that are supposed to drive the calculation of the $\vec{p}_{\mathrm{T}}^{\,\mathrm{miss}}$ vector. The M_{T2} variable is calculated using the algorithm discussed in Ref. [55]. With this definition, it has been shown that this variable has a kinematic endpoint at the mass of the W boson in the case of $\mathrm{t\bar{t}}$ events [56], while this is not true if extra invisible particles are present in the event. Since events with $M_{\mathrm{T2}} = 0$ GeV do not provide any discrimination power between signal and $\mathrm{t\bar{t}}$ background, only events with $M_{\mathrm{T2}} > 0$ GeV are used for hypothesis testing.

Figure 2 shows the M_{T2} distribution for signal and background, which are characterized by a slightly different shape for M_{T2} values smaller than 80 GeV and a large difference for $M_{\mathrm{T2}} >$ 80 GeV, due to the presence of the endpoint in the M_{T2} distribution for $\mathrm{t\bar{t}}$ events. This difference increases significantly when $\Delta m = m_{\tilde{\mathrm{t}}_1} - m_{\tilde{\chi}_1^0}$ is different from the top quark mass (Fig. 2 left). Furthermore, the differences in M_{T2} are large for signal points characterized by large neutralino masses, which add some extra $p_{\mathrm{T}}^{\mathrm{miss}}$ to the event (keeping $\Delta m = m_{\mathrm{top}}$, Fig. 2 right).

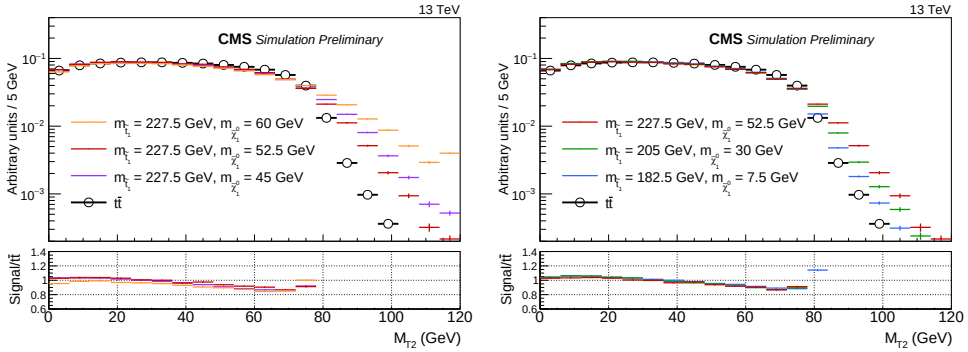

Figure 2: Normalized M_{T2} distributions using variables at generator level for $\mathrm{t\bar{t}}$ and simulated signal events with two generated leptons with p_{T} of at least 20 GeV and $|\eta| \leq 2.4$. The difference in the high values of M_{T2} increases significantly for points with $\Delta m = m_{\tilde{\mathrm{t}}_1}$ - $m_{\tilde{\chi}_1^0}$ is different from the top quark mass (left), or for signal models with higher neutralino masses when keeping $\Delta m = m_{\mathrm{top}}$ (right).

6 Background estimation

The $\mathrm{t\bar{t}}$ process accounts for approximately 94% of the total background yields in the selected region, and is modelled from MC simulation using the sample described in Section 3. For this modelling, a top quark mass of 172.5 GeV is assumed. The accurate knowledge of the $\mathrm{t\bar{t}}$ production process has been previously demonstrated in several cross section measurements by the CMS Collaboration [28, 54]. Also its differential cross section as a function of different variables has been measured [57] and MC parameters have been tuned using an independent data sample [38]. The main parameters affecting the $\mathrm{t\bar{t}}$ modelling and their associated uncertainties are discussed in Section 7. The tW background gives the second largest contribution, approximately 4%, and it is also modelled from MC simulation.

The contribution of events with jets misidentified as leptons or with leptons coming from the decay of a b quark mistakenly identified as coming from the hard process (nonprompt leptons) is estimated from data in a control region in which the electron and the muon are required to have equal charge (referred to as *same-sign*). This background is estimated using the observed events in the control region after subtraction of the prompt backgrounds estimated from MC (mainly from $\mathrm{t\bar{t}W}$ and $\mathrm{t\bar{t}Z}$ events or dileptonic $\mathrm{t\bar{t}}$ with a mismeasurement of the electron charge).

These events are weighted by the expected ratio of opposite-sign to same-sign events with nonprompt leptons; this ratio is estimated in MC simulation to be 1.2 ± 0.1.

Other background contributions are estimated using MC simulation and come from DY, dibosons (WW, WZ, and ZZ), $t\bar{t}W$ and $t\bar{t}Z$, for a total contribution of about 1%.

A good agreement between data and SM predictions after the full event selection and after the corrections described in Section 4 is observed within the uncertainties and shown in Fig. 3 for the lepton p_T, p_T^{miss}, and the angle between the leptons in the transverse plane ($\Delta\phi(e,\mu)$). The uncertainties considered are described in Section 7.

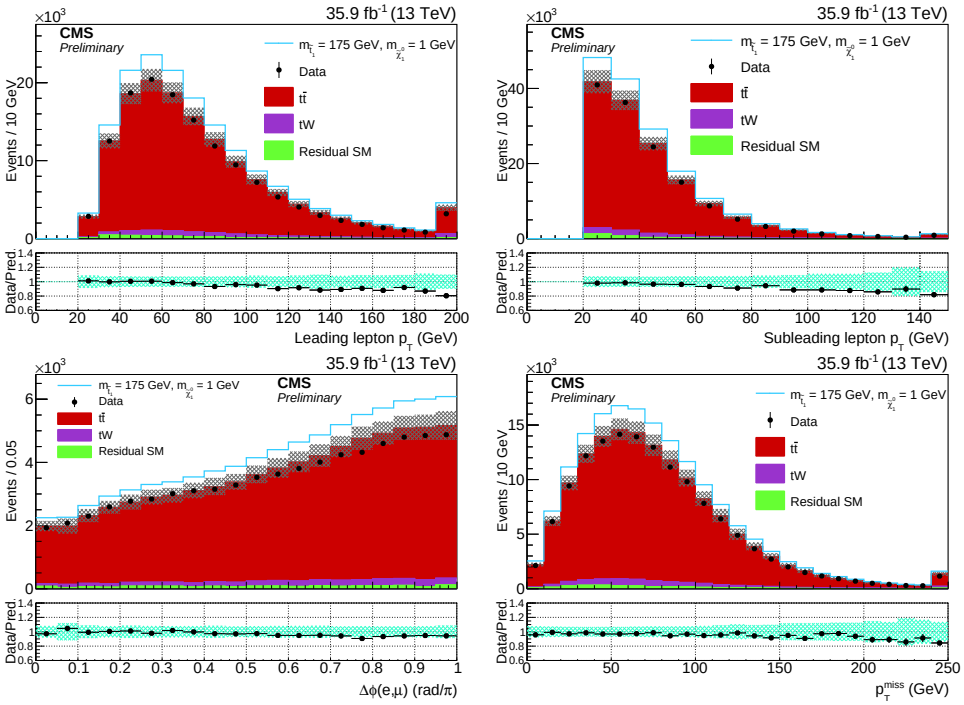

Figure 3: Distributions for leading and subleading lepton p_T, $\Delta\phi(e,\mu)$ and p_T^{miss}. The uncertainty band includes statistical and all systematic uncertainties described in Sec. 7. The last bin contains the overflow events.

7 Systematic uncertainties

Due to the large impact of the $t\bar{t}$ background prediction in this search, various modelling systematic uncertainties are assigned, reflecting the limited knowledge of the main theoretical parameters used in the simulation. The ranges of variation of these parameters were set in several previous CMS analysis [38] and the modelling of the $t\bar{t}$ background has been shown to accurately describe several kinematic variables within the uncertainties [57]. Details on the systematic uncertainties assigned due to modelling effects are detailed in Section 7.1.

The background and signal estimation are affected by several systematic uncertainties on acceptance, efficiency, and normalization. Uncertainties are considered on trigger efficiencies, lepton reconstruction, identification and isolation efficiencies, jet energy scale and resolution, pileup re-weighting, b tagging efficiency and mistagging efficiencies for every background and signal prediction. These uncertainties, described in Sec. 7.2, are assigned to each M_{T2} bin individually, and treated as correlated among all M_{T2} bins and all processes.

Some other uncertainties, including normalization uncertainties on tW and minor backgrounds and modelling uncertainties on signal, are described in Section 7.3.

7.1 Modelling uncertainties on $t\bar{t}$ background

An uncertainty of 6% is assigned to the $t\bar{t}$ background normalization, taking into account two effects. The first effect is the uncertainty on the NNLO calculation due to PDFs, α_S and scale using TOP++ for a top quark of 172.5 GeV [45] and the second effect is the uncertainty due to the choice of the top quark mass obtained by varying the top quark mass by ± 1 GeV in the calculation of the cross section.

On top of the normalization uncertainty, several sources of modelling uncertainties are considered. These uncertainties are treated as shape uncertainties and a summary of their effect on the $t\bar{t}$ acceptance is shown in Table 1.

The uncertainty in the modelling of the hard interaction process is assessed in the POWHEG sample through changes of μ_F and μ_R by factors of 2 and $\frac{1}{2}$ relative to their common nominal value of $Q^2 = m^2_{top} + p^2_{T,t}$. Here $p^2_{T,t}$ denotes the square transverse momentum of the top quark in the $t\bar{t}$ rest frame.

The uncertainty in the choice of the PDFs and in the value of α_s is determined by reweighting the sample of simulated $t\bar{t}$ events according to the envelope of a PDF set of 100 NNPDF3.0 replicas [58] and two extra replicas corresponding to variations of α_s by its uncertainties.

The impact of the modelling uncertainties of the initial and final state radiation is evaluated by varying the parton shower scales by factors of 2 and $\frac{1}{2}$ [31]. Also, the impact of the matrix element and parton shower matching, which is parameterized by the POWHEG as $h_{damp} = 1.58^{+0.66}_{-0.59} \cdot m_{top}$ [32], is calculated by varying this parameter within the uncertainties and propagating the result to the final yields.

The parameters of PYTHIA are tuned to model the measured underlying event [32, 38]. An uncertainty is assigned by varying these parameters within their uncertainties.

An uncertainty due to the limited knowledge on colour reconnection is estimated by comparing different models and taking the maximum variation with respect to the nominal value for each bin as the uncertainty. The procedure is described in detail in Ref. [32].

The top p_T in $t\bar{t}$ events has been found to be mismodelled [38]. A reweighting procedure, based on these studies, has been derived and the difference between the weighted and unweighted distributions is taken as an estimate of the uncertainty.

An uncertainty of 1.0 GeV in the top quark mass is also propagated to the acceptance. The differences in the M_{T2} yields for each bin of the distribution between $t\bar{t}$ prediction with $m_{top} = 172.5 \pm 1.0$ GeV are taken as an uncertainty, accounting for the possible bias introduced in the choice of $m_{top} = 172.5$ GeV on the MC simulation.

7.2 Experimental uncertainties

A summary of the effect of the experimental uncertainties on the M_{T2} distribution for events in the signal region is shown in Table 2.

The uncertainties in the dilepton trigger and lepton identification and isolation efficiencies in simulation are estimated by varying data-to-simulation scale factors by their uncertainties, which are about 1.5% for muon and electron identification and isolation, and about 0.5% for trigger uncertainty.

Table 1: Summary of modelling uncertainties on $t\bar{t}$ background, treated as shape uncertainties. The ranges correspond to variations of the uncertainty along the M_{T2} distribution. When only one number is shown, the uncertainty is approximately constant over the entire M_{T2} range.

Source	Range (%)
ME/PS matching (h_{damp})	0.3 – 2
Initial state radiation	0.5 – 1
Final state radiation	0.6 – 1.2
Color reconnection	≈ 1.5
ME scales	0.3 – 1
PDF	≈ 0.6
Top mass (acceptance)	≈ 1
Top p_T reweighting	0.1 – 0.5
Underlying event	≈ 0.8

To account for the uncertainties in the lepton energy scales, the energy of the leptons are varied by 0.2 GeV for muons and by about 0.1–0.5 GeV for electrons. The uncertainties associated with the jet energy scale and jet energy resolution are determined by varying such quantities in bins of p_T and η according to the uncertainties in the jet energy corrections, which amount to about a few percent.

The uncertainties due to the b tagging efficiency and mistagging rate are determined by varying the scale factors for b-tagged jets and light-flavour-tagged jets according to their uncertainties, as measured in $t\bar{t}$ events [50].

The uncertainty due to the pileup reweighting procedure is evaluated by varying the inelastic pp cross section by $\pm 4.6\%$ [59].

The uncertainty in p_T^{miss} due to the contribution of unclustered energy is evaluated based on the momentum resolution of the different PF candidates, according to their classification. Details on the procedure can be found in Ref. [47, 60, 61].

The uncertainty in the integrated luminosity, which affects the signal and background normalization, is currently estimated to be 2.5% [62].

Table 2: Summary of experimental uncertainties for $t\bar{t}$ and signal processes. The numbers represent typical values for the uncertainties on signal and $t\bar{t}$ yields or ranges for these uncertainties in different M_{T2} bins and different signal samples.

Source	Range for $t\bar{t}$ and signal (%)
Muon efficiencies	≈ 1.4
Electron efficiencies	≈ 1.5
Trigger efficiency	≈ 0.6
Lepton energy scale	0.5 – 2
Jet energy scale	1.5 – 3.0
Jet energy resolution	0.3 – 3.5
b-tagging efficiency	1.2 – 2.0
Mistagging efficiency	0.2 – 0.6
Unclustered p_T^{miss}	0.5 – 1.5
Pileup	0.5 – 3.5

7.3 Other uncertainties

A normalization uncertainty of 15% is applied to the DY process, covering differences seen between data and MC predictions in different jet multiplicity regions [54]. For other backgrounds, including tW, dibosons, and $t\bar{t}V$, a normalization uncertainty of 30% is assigned [54], covering the uncertainties in the predicted cross sections and possible extrapolation to the phase space used in the analysis. For the nonprompt lepton background, a normalization uncertainty of 30% is applied, taking into account the effect of the limited number of MC events used in the estimation of the same-sign to opposite-sign transfer factor applied, and the normalization of the prompt-process subtraction in the control region.

Furthermore, a 15% uncertainty in the signal normalization is assigned, according to the uncertainties in the predicted cross section of signal models in the top squark mass range on the analysis [46]. The effect on the acceptance of the uncertainties in factorization and renormalization scales is taken into account by varying μ_F and μ_R by factors of 2 and 0.5, respectively [63]. This uncertainty is propagated to the signal yields, resulting in a shape uncertainty of the order of 0.5–1.0% along the M_{T2} bins.

The MG5_aMC@NLO modelling of the initial state radiation is improved by scaling signal events according to a correction derived using $t\bar{t}$ events. An uncertainty is applied by considering variations of half the difference between the corrections and unity. The effect of this uncertainty on the signal yields amounts to about 1%, with individual values assigned to each M_{T2} bin.

8 Results

The predicted and observed M_{T2} distributions for selected events are shown in Fig. 4. No significant deviation from the SM is observed. The integrated expected and observed number of events are shown in Table 3. The result is interpreted in terms of the T2tt signal model from the Simplified Model Spectra [64, 65].

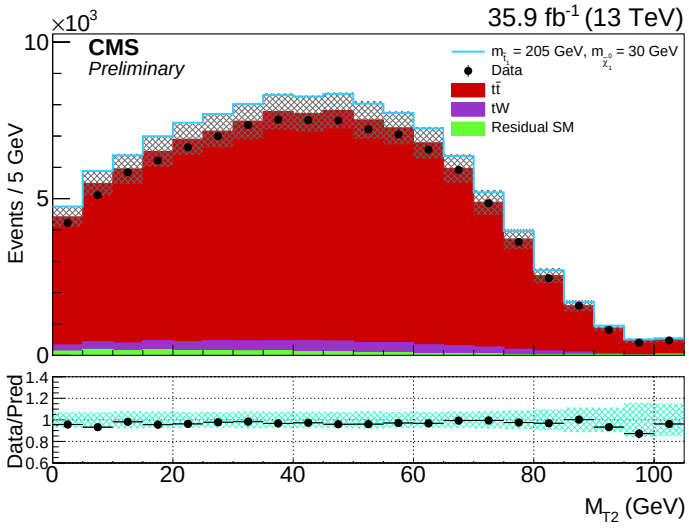

Figure 4: Expected and observed M_{T2} distribution for expected background and data. The M_{T2} distribution for a signal corresponding to a top squark mass of 205 GeV and a neutralino mass of 30 GeV is also shown, stacked on top of the background estimate. The hashed bands correspond to total systematic and statistical uncertainties.

Table 3: Number of expected and observed events after the selection with $M_{T2} > 0$ and $M_{T2} > 90$ GeV. The quoted uncertainties reflect both the statistical and systematic contributions.

Process	with $M_{T2} > 0$ GeV	with $M_{T2} > 90$ GeV
$t\bar{t}$	$102\,400 \pm 7400$	1680 ± 260
tW	4700 ± 1400	92 ± 32
Nonprompt leptons	1330 ± 400	30 ± 11
DY + $t\bar{t}$V+ Dibosons	570 ± 100	19 ± 6
Total Background	$109\,000 \pm 7600$	1821 ± 260
Signal: $m_{\tilde{t}_1} = 175.0$ GeV, $m_{\tilde{\chi}_1^0} = 1.0$ GeV	$16\,400 \pm 2500$	276 ± 53
Signal: $m_{\tilde{t}_1} = 205.0$ GeV, $m_{\tilde{\chi}_1^0} = 22.5$ GeV	8070 ± 1240	232 ± 41
Signal: $m_{\tilde{t}_1} = 205.0$ GeV, $m_{\tilde{\chi}_1^0} = 30.0$ GeV	7830 ± 1200	157 ± 27
Signal: $m_{\tilde{t}_1} = 205.0$ GeV, $m_{\tilde{\chi}_1^0} = 37.5$ GeV	6140 ± 650	262 ± 45
Signal: $m_{\tilde{t}_1} = 242.5$ GeV, $m_{\tilde{\chi}_1^0} = 67.5$ GeV	3550 ± 540	106 ± 19
Data	105 893	1694

The statistical interpretation is performed by testing the SM hypothesis against the SUSY hypothesis. A binned profile likelihood fit of the M_{T2} distribution is performed, where the nuisance parameters are modelled using log-normal priors. The results of the fit are shown in Fig. 4. Upper limits on the top squark pair production cross section are calculated at 95% confidence level (CL) using a modified frequentist approach and the CL_s criterion, implemented through an asymptotic approximation [66–69]. All the uncertainties in the background and signal predictions described in Section 7 are modelled as nuisance parameters and profiled in the fit.

We interpret the results for different signals characterized by top squark masses from 170 to 250 GeV and by three different mass differences between the top squark and the neutralino: $\Delta m(\tilde{t}_1, \tilde{\chi}_1^0) = 167.5$ GeV, 175.0 GeV, and 182.5 GeV. The sensitivity of the analysis to SUSY models with low neutralino masses and $\Delta m(\tilde{t}_1, \tilde{\chi}_1^0) = m_{top}$ comes mostly from the signal normalization, while the differences on M_{T2} shape become important for top squark masses greater than 210 GeV. For differences of masses of $\Delta m(\tilde{t}_1, \tilde{\chi}_1^0) = m_{top} \pm 7.5$ GeV the sensitivity of the analysis is mostly driven by the differences between the signal and $t\bar{t}$ distributions for high M_{T2} values ($M_{T2} \gtrsim 80$ GeV). The expected and observed upper limits are shown in Fig. 5.

We exclude the presence of a signal up to a top squark mass of 210 GeV for $|\Delta m(\tilde{t}_1, \tilde{\chi}_1^0)| - m_{top} = 0$ and up to top squark masses of 240 GeV for $|\Delta m(\tilde{t}_1, \tilde{\chi}_1^0) - m_{top}| = 7.5$ GeV.

9 Summary

A search for a top squark with mass close to the top quark mass is presented, using events with one opposite-sign electron-muon pair, at least two jets, and at least one b jet. The $\tilde{t}_1 \to t\tilde{\chi}_1^0$ decay mode is considered, and different top squark masses are explored up to 240 GeV with neutralino masses of $m_{\tilde{\chi}_1^0} \simeq m_{\tilde{t}_1} - m_{top}$.

An accurate estimation of the $t\bar{t}$ background, accounting for uncertainties due to all known theory and experimental effects, is crucial to be able to distinguish a signal that is expected to appear as an excess over the background expectation. The M_{T2} variable is used in a binned profile likelihood fit to increase the sensitivity thanks to the slightly different kinematics between the signal and the $t\bar{t}$ background. Further sensitivity is gained due to the absence of a kinematic endpoint in this variable for the signal, when top squark and neutralino mass difference

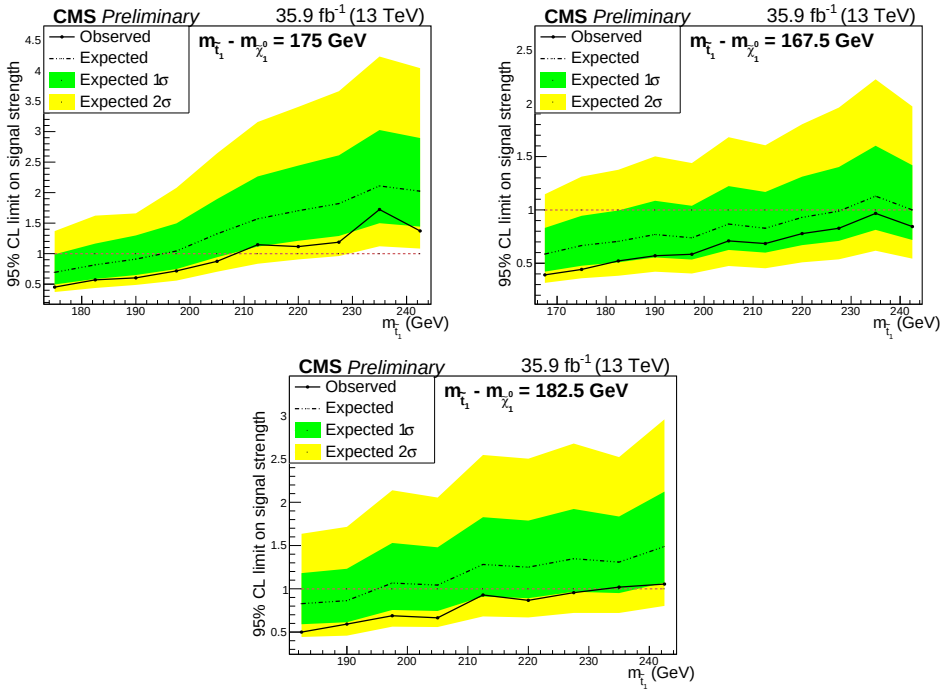

Figure 5: Expected and observed upper limits at 95% CL on the signal strength as a function of the top squark mass for $m_{\tilde{t}_1} - m_{\tilde{\chi}_1^0} = m_{\text{top}}$ (top left), $m_{\tilde{t}_1} - m_{\tilde{\chi}_1^0} = m_{\text{top}} + 7.5$ GeV (top right) and $m_{\tilde{t}_1} - m_{\tilde{\chi}_1^0} = m_{\text{top}} - 7.5$ GeV (bottom). The green and yellow bands correspond to the 1σ and 2σ ranges of the expected upper limits.

is greater than the top quark mass or when there are massive neutralinos in the event.

No excess is observed and upper limits are set at 95% CL on the top squark production cross section for top squark masses of up to 210 GeV in models with $m_{\tilde{t}_1} - m_{\text{top}} \simeq m_{\tilde{\chi}_1^0}$ and masses up to 240 GeV in models with a mass difference of 7.5 GeV. This result extends the exclusion limits of top squark searches at the LHC to higher top quark masses in the nearly degenerate region that was previously unexplored.

References

[1] R. Barbieri and G. F. Giudice, "Upper bounds on supersymmetric particle masses", *Nucl. Phys. B* **306** (1988) 63, doi:10.1016/0550-3213(88)90171-X.

[2] E. Witten, "Dynamical breaking of supersymmetry", *Nucl. Phys. B* **188** (1981) 513, doi:10.1016/0550-3213(81)90006-7.

[3] G. Bertone, D. Hooper, and J. Silk, "Particle dark matter: evidence, candidates and constraints", *Phys. Rept.* **405** (2005) 279, doi:10.1016/j.physrep.2004.08.031, arXiv:0404175.

[4] J. L. Feng, "Dark matter candidates from particle physics and methods of detection", *Ann. Rev. Astron. Astrophys.* **48** (2010) 495, doi:10.1146/annurev-astro-082708-101659, arXiv:1003.0904.

[5] P. Ramond, "Dual theory for free fermions", *Phys. Rev. D* **3** (1971) 2415, doi:10.1103/PhysRevD.3.2415.

[6] Y. A. Golfand and E. P. Likhtman, "Extension of the algebra of Poincaré group generators and violation of P invariance", *JETP Lett.* **13** (1971) 323.

[7] A. Neveu and J. H. Schwarz, "Factorizable dual model of pions", *Nucl. Phys. B* **31** (1971) 86, doi:10.1016/0550-3213(71)90448-2.

[8] D. V. Volkov and V. P. Akulov, "Possible universal neutrino interaction", *JETP Lett.* **16** (1972) 438.

[9] J. Wess and B. Zumino, "A lagrangian model invariant under supergauge transformations", *Phys. Lett. B* **49** (1974) 52, doi:10.1016/0370-2693(74)90578-4.

[10] J. Wess and B. Zumino, "Supergauge transformations in four-dimensions", *Nucl. Phys. B* **70** (1974) 39, doi:10.1016/0550-3213(74)90355-1.

[11] P. Fayet, "Supergauge invariant extension of the Higgs mechanism and a model for the electron and its neutrino", *Nucl. Phys. B* **90** (1975) 104, doi:10.1016/0550-3213(75)90636-7.

[12] H. P. Nilles, "Supersymmetry, supergravity and particle physics", *Phys. Rept.* **110** (1984) 1, doi:10.1016/0370-1573(84)90008-5.

[13] S. P. Martin, "A supersymmetry primer", *Adv. Ser. Direct. High Energy Phys.* **18** (1998) 1, doi:10.1142/9789812839657_0001, arXiv:hep-ph/9709356.

[14] G. R. Farrar and P. Fayet, "Phenomenology of the Production, Decay, and Detection of New Hadronic States Associated with Supersymmetry", *Phys. Lett. B* **76** (1978) 575, doi:10.1016/0370-2693(78)90858-4.

[15] R. K. Kaul and P. Majumdar, "Cancellation of quadratically divergent mass corrections in globally supersymmetric spontaneously broken gauge theories", *Nucl. Phys. B* **199** (1982) 36, doi:10.1016/0550-3213(82)90565-X.

[16] S. Dimopoulos and H. Georgi, "Softly broken supersymmetry and SU(5)", *Nucl. Phys. B* **193** (1981) 150, doi:10.1016/0550-3213(81)90522-8.

[17] ATLAS Collaboration, "Search for direct top squark pair production in final states with two leptons in $\sqrt{s} = 13$ TeV pp collisions with the ATLAS detector", *Eur. Phys. J. C* **77** (2017) 898, doi:10.1140/epjc/s10052-017-5445-x, arXiv:1708.03247.

[18] ATLAS Collaboration, "ATLAS Run 1 searches for direct pair production of third-generation squarks at the Large Hadron Collider", *Eur. Phys. J. C* **75** (2015) 510, doi:10.1140/epjc/s10052-015-3726-9, arXiv:1506.08616. [Erratum: doi:10.1140/epjc/s10052-016-3935-x].

[19] ATLAS Collaboration, "Search for top squark pair production in final states with one isolated lepton, jets, and missing transverse momentum in $\sqrt{s} = 8$ TeV pp collisions with the ATLAS detector", *JHEP* **11** (2014) 118, doi:10.1007/JHEP11(2014)118, arXiv:1407.0583.

[20] ATLAS Collaboration, "Search for direct top-squark pair production in final states with two leptons in pp collisions at $\sqrt{s} = 8$ TeV with the ATLAS detector", *JHEP* **06** (2014) 124, doi:10.1007/JHEP06(2014)124, arXiv:1403.4853.

[21] ATLAS Collaboration, "Search for top squarks in final states with one isolated lepton, jets, and missing transverse momentum in $\sqrt{s} = 13$ TeV pp collisions with the ATLAS detector", *Phys. Rev. D* **94** (2016) 052009, doi:10.1103/PhysRevD.94.052009, arXiv:1606.03903.

[22] CMS Collaboration, "Search for top squark pair production in pp collisions at $\sqrt{s} = 13$ TeV using single lepton events", *JHEP* **10** (2017) 019, doi:10.1007/JHEP10(2017)019, arXiv:1706.04402.

[23] CMS Collaboration, "Search for top squarks and dark matter particles in opposite-charge dilepton final states at $\sqrt{s} = 13$ TeV", *Phys. Rev. D* **97** (2018), no. 3, 032009, doi:10.1103/PhysRevD.97.032009, arXiv:1711.00752.

[24] CMS Collaboration, "Search for top-squark pair production in the single-lepton final state in pp collisions at $\sqrt{s} = 8$ TeV", *Eur. Phys. J. C* **73** (2013) 2677, doi:10.1140/epjc/s10052-013-2677-2, arXiv:1308.1586.

[25] CMS Collaboration, "Search for direct pair production of scalar top quarks in the single- and dilepton channels in proton-proton collisions at $\sqrt{s} = 8$ TeV", *JHEP* **07** (2016) 027, doi:10.1007/JHEP07(2016)027, arXiv:1602.03169. [Erratum: doi:10.1007/JHEP09(2016)056].

[26] CMS Collaboration, "Search for top squark pair production in compressed-mass-spectrum scenarios in proton-proton collisions at $\sqrt{s}$ = 8 TeV using the α_T variable", *Phys. Lett. B* **767** (2017) 403, doi:10.1016/j.physletb.2017.02.007, arXiv:1605.08993.

[27] CMS Collaboration, "Searches for pair production of third-generation squarks in $\sqrt{s} = 13$ TeV pp collisions", *Eur. Phys. J. C* **77** (2017) 327, doi:10.1140/epjc/s10052-017-4853-2, arXiv:1612.03877.

[28] CMS Collaboration, "Measurement of the $t\bar{t}$ production cross section in the eμ channel in proton-proton collisions at $\sqrt{s}$ = 7 and 8 TeV", *JHEP* **08** (2016) 029, doi:10.1007/JHEP08(2016)029, arXiv:1603.02303.

[29] ATLAS Collaboration, "Measurement of the $t\bar{t}$ production cross-section using $e\mu$ events with b-tagged jets in pp collisions at $\sqrt{s}$ = 7 and 8 TeV with the ATLAS detector", *Eur. Phys. J. C* **74** (2014) 3109, doi:10.1140/epjc/s10052-016-4501-2, arXiv:1406.5375. [Addendum: Eur. Phys. J.C76,no.11,642(2016)].

[30] CMS Collaboration, "The CMS experiment at the CERN LHC", *JINST* **3** (2008) S08004, doi:10.1088/1748-0221/3/08/S08004.

[31] S. Alioli et al., "A general framework for implementing NLO calculations in shower Monte Carlo programs: the POWHEG BOX", *JHEP* **06** (2010) 043, doi:10.1007/JHEP06(2010)043, arXiv:1002.2581.

[32] P. Skands, S. Carrazza, and J. Rojo, "Tuning PYTHIA 8.1: the Monash 2013 Tune", *Eur. Phys. J. C* **74** (2014) 3024, doi:10.1140/epjc/s10052-014-3024-y, arXiv:1404.5630.

[33] E. Re, "Single-top Wt-channel production matched with parton showers using the POWHEG method", *Eur. Phys. J. C* **71** (2011) 1547, doi:10.1140/epjc/s10052-011-1547-z, arXiv:1009.2450.

[34] J. Alwall et al., "The automated computation of tree-level and next-to-leading order differential cross sections, and their matching to parton shower simulations", *JHEP* **07** (2014) 079, doi:10.1007/JHEP07(2014)079, arXiv:1405.0301.

[35] R. Frederix and S. Frixione, "Merging meets matching in MC@NLO", *JHEP* **12** (2012) 061, doi:10.1007/JHEP12(2012)061, arXiv:1209.6215.

[36] T. Sjöstrand et al., "An Introduction to PYTHIA 8.2", *Comput. Phys. Commun.* **191** (2015) 159, doi:10.1016/j.cpc.2015.01.024, arXiv:1410.3012.

[37] NNPDF Collaboration, "Parton distributions for the LHC Run II", *JHEP* **04** (2015) 040, doi:10.1007/JHEP04(2015)040, arXiv:1410.8849.

[38] CMS Collaboration, "Investigations of the impact of the parton shower tuning in Pythia 8 in the modelling of $\mathrm{t\bar{t}}$ at $\sqrt{s} = 8$ and 13 TeV", CMS Physics Analysis Summary CMS-PAS-TOP-16-021, CERN, 2016.

[39] CMS Collaboration, "Event generator tunes obtained from underlying event and multiparton scattering measurements", *Eur. Phys. J. C* **76** (2016) 155, doi:10.1140/epjc/s10052-016-3988-x, arXiv:1512.00815.

[40] GEANT4 Collaboration, "GEANT4: A Simulation toolkit", *Nucl. Instrum. Meth. A* **506** (2003) 250, doi:10.1016/S0168-9002(03)01368-8.

[41] Y. Li and F. Petriello, "Combining QCD and electroweak corrections to dilepton production in the framework of the FEWZ simulation code", *Phys. Rev. D* **86** (2012) 094034, doi:10.1103/PhysRevD.86.094034, arXiv:1208.5967.

[42] N. Kidonakis, "Theoretical results for electroweak-boson and single-top production", *PoS* **DIS2015** (2015) 170, arXiv:1506.04072.

[43] J. M. Campbell, R. K. Ellis, and C. Williams, "Vector boson pair production at the LHC", *JHEP* **07** (2011) 018, doi:10.1007/JHEP07(2011)018, arXiv:1105.0020.

[44] M. Czakon, P. Fiedler, and A. Mitov, "Total Top-Quark Pair-Production Cross Section at Hadron Colliders Through O(α_S^4)", *Phys. Rev. Lett.* **110** (2013) 252004, doi:10.1103/PhysRevLett.110.252004, arXiv:1303.6254.

[45] M. Czakon and A. Mitov, "Top++: A Program for the Calculation of the Top-Pair Cross-Section at Hadron Colliders", *Comput. Phys. Commun.* **185** (2014) 2930, doi:10.1016/j.cpc.2014.06.021, arXiv:1112.5675.

[46] C. Borschensky et al., "Squark and gluino production cross sections in pp collisions at $\sqrt{s}$ = 13, 14, 33 and 100 TeV", *Eur. Phys. J. C* **74** (2014) 3174, doi:10.1140/epjc/s10052-014-3174-y, arXiv:1407.5066.

[47] CMS Collaboration, "Particle-flow reconstruction and global event description with the CMS detector", *JINST* **12** (2017) P10003, doi:10.1088/1748-0221/12/10/P10003, arXiv:1706.04965.

[48] M. Cacciari, G. P. Salam, and G. Soyez, "The anti-k_t jet clustering algorithm", *JHEP* **04** (2008) 063, doi:10.1088/1126-6708/2008/04/063, arXiv:0802.1189.

[49] M. Cacciari, G. P. Salam, and G. Soyez, "FastJet user manual", *Eur. Phys. J. C* **72** (2012) 1896, doi:10.1140/epjc/s10052-012-1896-2, arXiv:1111.6097.

[50] CMS Collaboration, "Identification of heavy-flavour jets with the CMS detector in pp collisions at 13 TeV", *JINST* **13** (2018) 05011, doi:10.1088/1748-0221/13/05/P05011, arXiv:1712.07158.

[51] CMS Collaboration, "Performance of CMS muon reconstruction in pp collision events at $\sqrt{s} = 7$ TeV", *JINST* **7** (2012) P10002, doi:10.1088/1748-0221/7/10/P10002, arXiv:1206.4071.

[52] CMS Collaboration, "Performance of electron reconstruction and selection with the CMS detector in proton-proton collisions at $\sqrt{s} = 8$ TeV", *JINST* **10** (2015) P06005, doi:10.1088/1748-0221/10/06/P06005, arXiv:1502.02701.

[53] CMS Collaboration, "Performance of missing energy reconstruction in $\sqrt{s} = 13$ TeV pp collision data using the CMS detector", CMS Physics Analysis Summary CMS-PAS-JME-16-004, CERN, 2016.

[54] CMS Collaboration, "Measurement of the $t\bar{t}$ production cross section using events in the eμ final state in pp collisions at $\sqrt{s} = 13$ TeV", *Eur. Phys. J. C* **77** (2017) 172, doi:10.1140/epjc/s10052-017-4718-8, arXiv:1611.04040.

[55] H.-C. Cheng and Z. Han, "Minimal Kinematic Constraints and MT2", *JHEP* **12** (2008) 063, doi:10.1088/1126-6708/2008/12/063, arXiv:0810.5178.

[56] C. G. Lester and D. J. Summers, "Measuring masses of semi-invisibly decaying particles pair produced at hadron colliders", *Phys. Lett. B* **463** (1999) 99, doi:10.1016/S0370-2693(99)00945-4, arXiv:hep-ph/9906349.

[57] CMS Collaboration, "Measurements of differential cross sections of top quark pair production as a function of kinematic event variables in proton-proton collisions at $\sqrt{s} = 13$ TeV", *JHEP* **06** (2018) 002, doi:10.1007/JHEP06(2018)002, arXiv:1803.03991.

[58] J. Gao et al., "CT10 next-to-next-to-leading order global analysis of QCD", *Phys. Rev. D* **89** (2014) 033009, doi:10.1103/PhysRevD.89.033009, arXiv:1302.6246.

[59] ATLAS Collaboration, "Measurement of the Inelastic Proton-Proton Cross Section at $\sqrt{s} = 13$ TeV with the ATLAS Detector at the LHC", *Phys. Rev. Lett.* **117** (2016) 182002, doi:10.1103/PhysRevLett.117.182002, arXiv:1606.02625.

[60] CMS Collaboration, "Performance of photon reconstruction and identification with the CMS detector in proton-proton collisions at $\sqrt{s} = 8$ TeV", *JINST* **10** (2015) P08010, doi:10.1088/1748-0221/10/08/P08010, arXiv:1502.02702.

[61] CMS Collaboration, "Description and performance of track and primary-vertex reconstruction with the CMS tracker", *JINST* **9** (2014) P10009, doi:10.1088/1748-0221/9/10/P10009, arXiv:1405.6569.

[62] CMS Collaboration, "CMS Luminosity Measurements at 13 TeV — Winter 2017 Update", CMS Physics Analysis Summary CMS-PAS-LUM-17-001, CERN, 2017.

[63] A. Kalogeropoulos and J. Alwall, "The SysCalc code: A tool to derive theoretical systematic uncertainties", arXiv:1801.08401.

[64] J. Alwall, P. Schuster, and N. Toro, "Simplified Models for a First Characterization of New Physics at the LHC", *Phys. Rev. D* **79** (2009) 075020, doi:10.1103/PhysRevD.79.075020, arXiv:0810.3921.

[65] LHC New Physics Working Group Collaboration, "Simplified Models for LHC New Physics Searches", *J. Phys. G* **39** (2012) 105005, doi:10.1088/0954-3899/39/10/105005, arXiv:1105.2838.

[66] G. Cowan, K. Cranmer, E. Gross, and O. Vitells, "Asymptotic formulae for likelihood-based tests of new physics", *Eur. Phys. J. C* **71** (2011) 1554, doi:10.1140/epjc/s10052-011-1554-0, arXiv:1007.1727. [Erratum: doi:10.1140/epjc/s10052-013-2501-z].

[67] T. Junk, "Confidence level computation for combining searches with small statistics", *Nucl. Instr. Meth. A* **434** (1999) 435, doi:10.1016/S0168-9002(99)00498-2, arXiv:hep-ex/9902006.

[68] A. L. Read, "Presentation of search results: the CL_s technique", in *Durham IPPP Workshop: Advanced Statistical Techniques in Particle Physics*, p. 2693. Durham, UK, March, 2002. J. Phys. G 28 (2002) 2693. doi:10.1088/0954-3899/28/10/313.

[69] The ATLAS Collaboration, The CMS Collaboration, The LHC Higgs Combination Group, "Procedure for the LHC Higgs boson search combination in Summer 2011", Technical Report CMS-NOTE-2011-005. ATL-PHYS-PUB-2011-11, CERN, 2011.